AIAA JOURNAL
Vol. 39, No. 7, July 2001

Fluorescence Visualization of Hypersonic Flow Establishment over a Blunt Fin

J. S. Fox,* S. O'Byrne,* and A. F. P. Houwing†
Australian National University, Acton, Australian Capital Territory 0200, Australia
A. Papinniemi‡
University of New South Wales, Campbell, Australian Capital Territory 2612, Australia
P. M. Danehy§
NASA Langley Research Center, Hampton, Virginia 23681-2199
and
N. R. Mudford¶
University of New South Wales, Campbell, Australian Capital Territory 2612, Australia

Fluorescence imaging is used to investigate the separated flow upstream of a blunt fin in a hypersonic freestream with a transitional boundary layer. Images are presented to show the flow development before, during, and after the test time of the free-piston shock tunnel used to generate the flow. These images indicate that the test time in this facility is long enough to achieve a steady flow over the blunt fin. Thermocouple measurements are included to compare the surface heat flux upstream of the fin with that for flow along a flat plate with the same freestream conditions. The heat flux results are consistent with separation in a transitional boundary layer and show that the separated flow is oscillatory.

Nomenclature

a	=	sound speed, $\mathrm{m}\cdot\mathrm{s}^{-1}$
a_δ	=	average sound speed in boundary layer, $\mathrm{m}\cdot\mathrm{s}^{-1}$
C_f	=	skin-friction coefficient
d	=	fin diameter, m
d_1	=	separation length, m
h_e	=	specific enthalpy of freestream, $\mathrm{J}\cdot\mathrm{kg}^{-1}$
h_w	=	specific enthalpy at wall, $\mathrm{J}\cdot\mathrm{kg}^{-1}$
h_1	=	verticle distance from plate to triple point, m
h_2	=	vertical distance from plate to shear layer below triple point, m
L	=	length of flat plate, m
l_{sep}	=	separation length, m
M	=	Mach number
M_∞	=	Mach number in freestream
Pr	=	Prandtl number
$p_{\mathrm{pitot},\infty}$	=	pitot pressure, Pa
p_0	=	nozzle reservoir pressure, Pa
$\dot{q}_s(t)$	=	surface heat flux, $\mathrm{J}\cdot\mathrm{m}^{-2}\cdot\mathrm{s}^{-1}$
R	=	gas constant, $\mathrm{J}/(\mathrm{kg}\cdot\mathrm{K})$
Re	=	Reynolds number
St	=	Stanton number based on freestream conditions
T	=	temperature, K
T_w	=	temperature at wall, K
T_∞	=	temperature in freestream, K
T^*	=	Eckert reference temperature, K
t	=	time, s
U	=	velocity, $\mathrm{m}\cdot\mathrm{s}^{-1}$
U_∞	=	flow speed ahead of the bow shock, $\mathrm{m}\cdot\mathrm{s}^{-1}$
u_e	=	velocity of freestream, $\mathrm{m}\cdot\mathrm{s}^{-1}$
X	=	position at which Δt_{NT} is evaluated, m
x	=	distance from nozzle throat along nozzle axis, m
α_1	=	angle of separation shock with horizontal, deg
α_2	=	angle of shear layer with horizontal, deg
α_λ	=	angle of lambda shock with horizontal, deg
γ	=	ratio of specific heats
γ_∞	=	ratio of specific heats in freestream
Δ	=	asymptotic value of shock standoff distance, m
Δt_E	=	time to establish overall flow, s
$\Delta t_{E,\max}$	=	maximum time to establish overall flow, s
$\Delta t_{E,\min}$	=	minimum time to establish overall flow, s
$\Delta t_{\mathrm{nozzle}}$	=	time to establish nozzle flow, s
Δt_{NT}	=	time for sound waves to travel through nozzle, s
Δ'	=	shock standoff distance when established, m
ρ_e	=	density of freestream, $\mathrm{kg}\cdot\mathrm{m}^3$
ρ_s	=	density behind bow shock, $\mathrm{kg}\cdot\mathrm{m}^3$
ρ_∞	=	density ahead of bow shock, $\mathrm{kg}\cdot\mathrm{m}^3$
τ_{bl}	=	characteristic response time (boundary layer), s
τ_{bs}	=	characteristic response time (bow shock), s
τ_{sep}	=	characteristic response time (separated flow), s

Received 6 June 2000; revision received 2 January 2001; accepted for publication 25 January 2001.

*Graduate Student, Aerophysics and Laser-Based Diagnostics Research Laboratory, Department of Physics and Theoretical Physics. Student Member AIAA.

†Associate Professor, Aerophysics and Laser-Based Diagnostics Research Laboratory, Department of Physics and Theoretical Physics. Member AIAA.

‡Graduate Student, Department of Aerospace and Mechanical Engineering, University College.

§Research Scientist, Instrumentation Systems Development Branch, MS 236. Member AIAA.

¶Senior Lecturer, Department of Aerospace and Mechanical Engineering, University College. Member AIAA.

Introduction

AERODYNAMIC heating is one of the critical problems in the design of high-speed aerospace vehicles. High thermal stresses occur in vehicles around the nose region, on leading edges, and in corner regions, such as in the junctions between wing and body, fin and body, pylon and wing, fin and wing, and flap and wing. In addition, the intake ducts of airbreathing engines can be subject to high thermal loads resulting from shock–shock and shock–vortex interactions. A number of important viscous interaction problem regions have been identified[1,2]: leading-edge shock impingement, fin interaction, flap deflection, axial corner flows, and a number of other shock-wave/boundary-layer interaction problems. This paper investigates one of these problems, the fin interference problem, in which a shock-wave/boundary-layer interaction induces flow separation.

Figure 1 shows the main features of hypersonic flow over a blunt fin on a flat plate. The bow shock upstream of the fin generates a pressure rise, which is communicated upstream through the subsonic portion of the boundary layer, causing the flow on the flat plate to

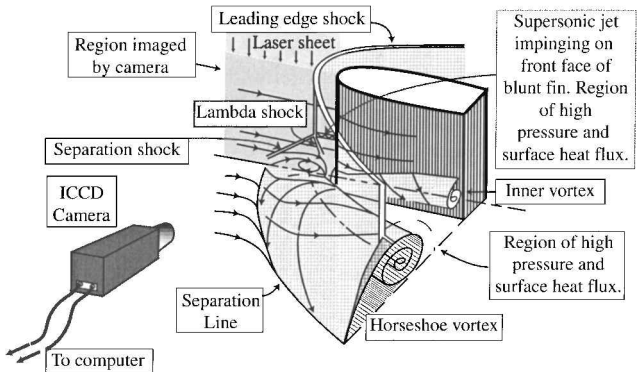

Fig. 1 Schematic of the three-dimensional flow around a blunt fin (after Stollery[5]).

separate and deflect away from the fin. Stollery[2] has discussed the flow features in the three-dimensional flowfield near an unswept blunt-nosed strut (or blunt fin). The primary flow feature associated with the diversion of flow around the fin is a horseshoe vortex,[3,4] which forms upstream of the fin. Theory predicts the presence of two vortices in this model of the flow, but as many as six vortices have been indicated by surface oil patterns in some cases.[5] In experiments, maximum pressures and heat flux rates occur near the reattachment lines associated with these vortices.[3]

The problems associated with attempting to visualize the fin interaction flows are twofold. First, optical access for traditional line-of-sight visualization techniques, such as shadowgraph, schlieren, or interferometry, is severely restricted by the presence of the surfaces that make up the fin–body junction. Second, even if optical access is achieved, line-of-sight methods, which are strictly suitable for two-dimensional flows only, will not be able to resolve the highly three-dimensional features.

To date, the flowfield structure for this type of flow has been inferred largely from surface gauge measurements or surface visualization techniques such as the sublimation method, oil flow techniques, laser interferometer skin-friction technique, infrared thermography, and liquid crystal thermography.[6–10] Flowfield visualization, other than line-of-sight visualization, has been restricted to the electron beam method,[11] which is confined to low-density flows, and planar laser scattering[12] requiring seeding with particles, which may lag behind fluid particles in their motion.

The restrictions of optical access and the problems associated with the visualization of a three-dimensional flowfield can be overcome by using planar laser-induced fluorescence (PLIF). PLIF can provide comprehensive flowfield visualization of the supersonic fin interaction flow, as well as valuable information against which theoretical models and computational fluid dynamics (CFD) calculations can be tested.[13] At present, CFD rarely predicts the complex flows created by the interaction between boundary layers, separation shocks, reattachment shocks, free shear layers, and other flow features accurately.[14–16] When PLIF visualization is used, the position and shape of these flow features can be determined experimentally, thus providing simple parameters, such as the location of the separation point and the angle of the separation shock, which can be directly compared to CFD calculations.

This paper describes a series of PLIF flow visualization and heat flux measurements that determine whether the separated flow upstream of a blunt-fin model geometry reaches a steady state during the test time available in a free-piston shock tunnel.[17] Free-piston shock tunnels are pulsed facilities that can be used to generate a wide range of hypersonic flow conditions. A major difficulty associated with their use is their extremely short flow duration. This problem becomes particularly serious when examining separated flows, such as in the blunt-fin problem, because the time required for flow to establish in the separated region is significantly longer than the other flow features of interest such as bow shocks and attached boundary layers. The steady flow test time in such a facility is the time interval between the establishment of steady test-gas flow in the nozzle and the arrival of the driver gas. Depending on the conditions required in the test section, the test time can range from 100 μs to 4 ms. Previous work using PLIF visualization[18] has shown that a steady flow in the near wake of a cone can be achieved during the test time available to a small free-piston shock tunnel.

Flow Establishment

For the purposes of the following discussion, we define Δt_{nozzle} as the time taken to establish steady nozzle flow at the model station together with time constants τ_{bl}, τ_{sep}, and τ_{bs}, which are the characteristic times for response of the boundary layer, separated flow, and bow shock on the blunt fin, respectively, to changes in the freestream flow. These characteristic times may be evaluated as the times taken for each flow feature to reach its steady state after impulsive exposure of a body to a steady freestream flow. As will be discussed, the literature contains empirical expressions for evaluating these times. The question to be addressed, then, is at what time Δt_E after incident primary shock reflection does the model flow become stationary? Here, the term stationary is used in the same sense as in turbulence studies, that is, although flow quantities may fluctuate over the short term, their long-term means are constant.

Mallinson et al.[19] stated that a conservative estimate of Δt_E in a compression corner may be obtained as the sum of Δt_{nozzle}, τ_{bl}, and τ_{sep}. This estimate assumes that the flow features develop serially. The conservative nature of this assumption derives from that, in reality, all of the flow features will need to respond to flow changes that occur while the nozzle flow is being established and that interactions between the inviscid flow, boundary layer, and separated region may continue sometime after the nozzle flow has established. An additional contributor to the conservative margin is the division of the separated flow into boundary layer, separated flow region, and bow shock. Were the combination to be considered as a single flow feature, then it would have a single characteristic time appropriate to the simultaneous development of the three individual features as discerned here. However, following Mallinson, we take the sum of Δt_{nozzle}, τ_{bl}, τ_{sep}, and τ_{bs} as a useful upper limit for flow establishment time. That is,

$$\Delta t_{E,\max} = \Delta t_{\text{nozzle}} + \tau_{\text{bl}} + \tau_{\text{sep}} + \tau_{\text{bs}} \tag{1}$$

In the case where all of τ_{bl}, τ_{sep}, and τ_{bs} are much less than Δt_{nozzle}, we may argue that the boundary layer, separated flow region, and bow shock respond quickly enough to freestream flow changes to allow us to make the approximation that the nozzle establishment time is a useful minimum for the flow establishment time. That is,

$$\Delta t_{\text{E,min}} \approx \Delta t_{\text{nozzle}} \tag{2}$$

We now proceed to find approximations for Δt_{nozzle}, τ_{bl}, τ_{sep}, and τ_{bs}, for the present flow, to determine values for $\Delta t_{E,\max}$ and $\Delta t_{E,\min}$, plus examine the reasonableness of this last approximation.

Nozzle Flow Establishment

The starting process in a supersonic nozzle has been studied extensively in previous work.[20,21] It is initiated when the primary incident shock in the shock tube is reflected at the shock tube end wall and the first test gas passes into the nozzle. Much of the earlier work on nozzle flow establishment deals with planar two-dimensional nozzle flows. However, the qualitative features of the axisymmetric case are expected to be similar. From this early work, the nozzle flow evolution is known to be a complicated process involving multiple shock and boundary-layer interactions.[21] In fact, it is so complicated, that it is well nigh impossible to quantify Δt_{nozzle} on the basis of fluid mechanical theory. Consequently, Δt_{nozzle} is determined experimentally here, as will be described.

For a perfect gas flow, the test section flow can be considered to be steady when the Mach number of the flow is constant. Boyce et al.[22] argue that the Mach number is steady in flows with changing nozzle reservoir pressure p_0 when the ratio of the freestream pitot pressure $p_{\text{pitot},\infty}(t)$ at a time t to the nozzle reservoir pressure $p_0(t - \Delta t_{NT})$ at an earlier time $t - \Delta t_{NT}$ is constant. Here the nozzle transit time Δt_{NT} is the time taken for acoustic disturbances to travel from the nozzle reservoir to the test section:

$$\Delta t_{NT} = \int_{x=0}^{x=X} \frac{\mathrm{d}x}{U+a} \tag{3}$$

where x is the distance from the throat along the nozzle centerline, X is the position at which Δt_{NT} is evaluated, U is the local flow velocity, and is a the local speed of sound. The parameters U and a can be calculated using the one-dimensional nonequilibrium nozzle code STUBE.[23]

Additionally, in the case of steady nozzle flow of a perfect gas,

$$\frac{p_{\text{pitot},\infty}(t)}{p_0(t-\Delta t_{NT})} = \left[1+\frac{2\gamma}{\gamma+1}(M^2-1)\right]^{-1/(\gamma-1)} \times \left[\frac{(\gamma+1)M^2}{(\gamma-1)M^2+2}\right]^{\gamma/(\gamma-1)} \tag{4}$$

where M is the Mach number of the flow just upstream of the pitot probe. Hence, the ratio of the pitot and nozzle reservoir pressures can also be used to give an indication of the Mach number of the flow at any given time after shock reflection, if γ is known. The nozzle flow behaves as if γ is close to 1.4, consistent with this being a low enthalpy flow condition. However, the bow shock generated around the pitot probe elevates the temperature, which decreases the effective γ to about 1.33. Hence, $\gamma = 1.33$ is used in this equation.

Establishment of Steady Attached Boundary-Layer Flow

Davies and Bernstein[24] found that the characteristic time to achieve a steady attached boundary layer on a flat plate, τ_{bl}, is given by

$$\tau_{\text{bl}} = 3.33L/U_\infty \tag{5}$$

where U_∞ is the freestream flow velocity.

Establishment of Steady Shear Layer Downstream of Separation

The characteristic time to establish a separated flow on a compression corner, τ_{sep}, was calculated by Holden[25] using

$$\tau_{\text{sep}} = l_{\text{sep}}/\bar{a}_\delta = d_1/\bar{a}_\delta \tag{6}$$

where l_{sep} is the separation length (d_1 in our work) and a_δ is the average sound speed in the boundary layer. We will assume that this equation can be also used for the characteristic time to establish the separated flow produced on the blunt fin. The assumption underlying this formulation is that the dimensions and flow within the separated flow region are set by means of an acoustic wave that emanates from the fin and travels forward to the steady flow separation point. The average speed of sound in the boundary layer, a_δ, can be determined using an intermediate temperature such as the Eckert temperature T^* (Ref. 26), where

$$T^* = 0.5(T_w + T_\infty) + 0.11(Pr)^{\frac{1}{2}}(\gamma_\infty - 1)M_\infty^2 T_\infty \tag{7}$$

Here T_w is assumed to be 300 K, Pr is assumed to have a value of 0.72, γ_∞ is the freestream ratio of specific heats, which, for these experiments, is close to a value of 1.4. When ideal-gas behavior is assumed, a_δ can be written as

$$\bar{a}_\delta = \sqrt{\gamma_\infty R T^*} \tag{8}$$

In this work, we estimate the length of the separation region from the flow visualization by extrapolating the separation shock to the point at which it would intersect the flat plate and measuring the distance from that point to the corner of the blunt fin. This method has been used in a previous schlieren visualization study of turbulent blunt fin flow.[27] Other flow parameters required for the calculation are determined from the computer code STUBE,[23] used to calculate the steady nozzle flow.

Establishment Time for Bow Shock

Miles et al.[28] derived the following equation for the time to establish a bow shock at the front of a circular cylinder:

$$\tau_{\text{bs}} = \Delta/U_\infty[(\rho_s/\rho_\infty) - 1]\,\ell n[1-(\Delta'/\Delta)]^{-1} \tag{9}$$

where U_∞ is the flow speed ahead of the bow shock and Δ' is the value of the shock standoff distance when the bow shock is considered to be established. In our work, we will consider the bow shock to be established when the standoff distance has reached 95% of its asymptotic value. That is, $\Delta'/\Delta = 0.95$. In the case of perfect gas flow over a cylinder of diameter d, mass flux considerations and experimental data show that Δ is given by the following formula[29]:

$$\Delta/d = 1.16(\rho_\infty/\rho_S) \tag{10}$$

Experimental Method

Flow Conditions

Experiments were performed in the T3 free-piston shock tunnel at the Australian National University.[17] A 305-mm-exit-diameter axisymmetric conical nozzle with a 35-mm-diam throat and 7.5-deg internal half-angle was used to expand gas at a stagnation temperature and pressure of 3480 K and 15.9 MPa, respectively, over a blunt fin model mounted on the centerline of a flat plate. Because of the conical geometry of the nozzle, the freestream flow can be approximated as a source flow. A slight flow divergence causes the Mach number of the freestream to vary from a value of approximately 6.1 at the leading edge of the flat plate to 6.9 at the location of the blunt fin.

The shock tube fill condition of 2% O_2 in N_2, selected to generate the required amount of NO for good fluorescence imaging, results in a test gas composition of 1.6% NO, 1.2% O_2, 0.06% O, and 97.14% N_2 by mole fraction at the nozzle exit (calculated using STUBE[23]). The Mach number, temperature, and pressure of the freestream were 6.4 ± 0.1, 446 ± 5 K, and 7.2 ± 0.4 kPa, respectively; the stagnation enthalpy was 3.90 ± 0.02 MJ/kg. The unit Reynolds number at these conditions is 5.9×10^6 m^{-1}. Based on previous work,[30] we assume a transition Reynolds number of 1.0×10^6, which indicates that transition should occur approximately 170 mm from the leading edge of the flat plate, that is, 155 mm, or 3.9 fin diameters, upstream of the fin.

Model and Instrumentation

The flat plate is shown schematically in Fig. 2. It was mounted on a sting positioned so that the top surface was in the center of the nozzle flow. The blunt fin was attached perpendicularly to the flat plate; it was not swept and was at a zero angle of attack. Before the experiment, the leading edge of the flat plate was inserted 160 mm inside the nozzle such that the fin was 163 mm downstream of the nozzle exit. During the experiment, the shock tunnel recoils by about 30 mm away from the model. The blunt fin is 38 mm thick with a hemicylindrical nose. The height of the blunt fin was 100 mm, which is high enough to be considered as semi-infinite, so that any increases in height of the blunt fin would not affect the flow.

Coaxial chromel–alumel thermocouples, of 2.3-mm outer diameter, were used to obtain the heat flux measurements. Four of these were flush mounted along the centerline of the plate, at the positions indicated in Fig. 2. For the remainder of the discussion, the thermocouples are labeled TC1–TC4, in order of increasing distance downstream of the leading edge of the plate. They were placed so that TC1 was in the undisturbed flat plate boundary-layer flow, TC2 was located near the separation point, and TC3 and TC4 were within the separated region and within the area illuminated by the laser sheet. The blunt fin is 323 mm from the leading edge of the flat

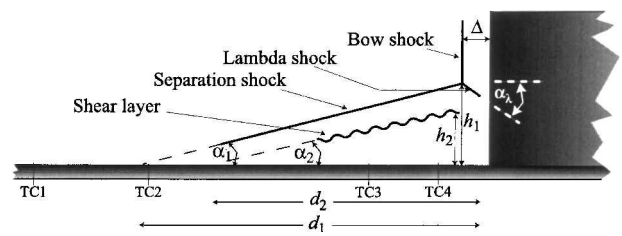

Fig. 2 Side view schematic of the blunt fin attached to a flat plate with the expected flow features and positions of the thermocouples.

Table 1 Calculated establishment times for flow processes, calculated for three different positions in the flow

Position in flow	x, mm	Δt_{NT} μs	Δt_{nozzle}, μs	τ_{bl}, μs	τ_{bs}, μs	τ_{sep}, μs	$\Delta t_{E,\min}$, μs	$\Delta t_{E,\max}$, μs
Leading edge of plate	870	305	1450	401	40	226	1450	2117
Exit of nozzle	1030	359	1500	404	40	228	1500	2172
Blunt fin model	1195	419	1560	399	40	230	1560	2229

plate, whereas thermocouples TC1, TC2, TC3, and TC4 are 113, 170, 274, and 307 mm, respectively, from the leading edge.

The thermocouples were produced in-house and have been used successfully in previous measurements performed for a hypersonic compression-corner flow.[19] Although less sensitive than thin-film gauges, thermocouples are less susceptible to damage arising from diaphragm fragments or the high levels of heat flux that can occur just upstream of the fin. The thermocouple voltages were amplified using a 30-dB differential preamplifier and recorded by two Tektronix TDS 310 digital oscilloscopes.

Pitot and Nozzle Reservoir Pressure Measurements

Before the blunt fin experiments, the flow conditions were characterized by measuring the pitot pressure at the exit of the nozzle and comparing it with the nozzle reservoir pressure as already described. The pitot probe was placed at the exit of the nozzle and along the centerline of the flow.

PLIF Excitation and Detection

The PLIF method is a well-established flow imaging technique that can be used to measure static temperature[31] and pressure,[32] perform species imaging,[33,34] and for flow visualization.[18] In the current work, we used the $R_2(13.5)$ transition in the $A^2\Sigma \leftarrow X^2\Pi(0, 0)$ band of NO, determined from previous work[35] to be a good transition for qualitatively visualizing the important flow features. A sheet of laser light tuned to this transition illuminated the plane of symmetry shown in Figs. 1 and 2. The resultant fluorescence from laser-excited NO molecules in the illuminated plane was imaged by an intensified charge-coupled device camera as shown in Fig. 1. Luminosity from flow contaminants[36] reduces the signal to noise ratio, and for that reason we used a short camera gate of approximately 100 ns. This gate was long enough to capture over 90% of the fluorescence while short enough to reject the majority of the natural flow luminosity. A more detailed description of the optical setup is provided by Fox et al.[33]

Results

The results of the calculations for the establishment time of different flow processes at the leading edge of the flat plate, at the exit of the nozzle, and at the blunt fin model are shown in Table 1. The characteristic times of the establishment of bow shock, separated region, and boundary layer are, indeed, significantly smaller than Δt_{nozzle}, which indicates we may be justified in making the approximation $\Delta t_E = \Delta t_{E,\min} = \Delta t_{\text{nozzle}}$.

Determination of Nozzle Flow Startup Time

The result of the calculation for the ratio of pitot pressure to nozzle reservoir pressure is shown in Fig. 3 with the nozzle reservoir and pitot pressure traces. A constant value is reached at about 1.5 ms, which agrees well with results from previous work,[22] and is consistent with a perfect gas flow having a Mach number of 6.4 and an effective value of 1.33 for the ratio of specific heats.

PLIF Imaging of Flow Development

Figure 4 shows PLIF images, corrected for spatial variation in the profile of the laser sheet, taken at different delay times and shows how the flow develops. Each image is obtained during successive runs of the tunnel, and therefore, the images will be subject to some variation due to the nonrepeatability of the turbulent structures. The datum for all times is the time of the reflection of the primary incident shock in the shock tube. In all images the flow is from left to right, and the laser enters from the top of the image. Each image is

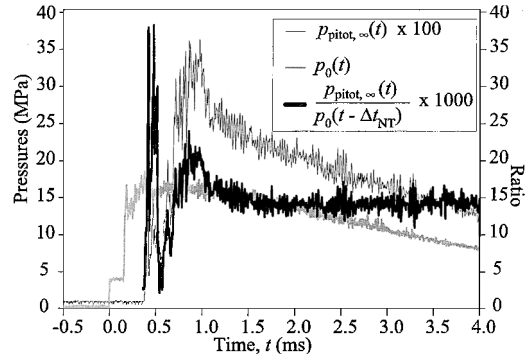

Fig. 3 Nozzle reservior pressure trace and freestream pitot pressure trace shown with the ratio of pitot to reservoir pressures at this 4 MJ/kg condition; time when steady nozzle flow was established is the time when this pressure ratio first becomes constant.

75 ± 1 mm wide and 55 ± 1 mm high. The right-hand edge of each image corresponds to the position of the blunt fin. The images are displayed in grayscale using a logarithmic scale, with light shades corresponding to high signals and dark shades to low signals.

Some features of the nozzle startup processes are seen in Fig. 4a at a time of 250 μs. The nozzle starting shock is apparent as a sudden change in intensity near the fin. This feature is similar to that reported in the schlieren images of Smith.[20] In this image, the nozzle shear layer is visible, indicating that the nozzle flow is not yet established. At a later time of 400 μs, as shown in Fig. 4b, the flow begins to show the presence of the separation shock. However, the bow shock is still not properly formed and the shear layer appears laminar. At the top of the image, the nozzle shear layer is still visible. As seen by the disturbance in the bow shock near the top of the blunt fin, the bow shock appears to interact with the nozzle shear layer in some way at a time of 600 μs (see Fig. 4c). At this time, turbulent structures become visible in the separated region. The separation-shock/bow-shock interaction is now strong enough to form a lambda shock. Between 400 and 800 μs (see Figs. 4b–4d), the separation point moves downstream until, by 800 μs, it is within the field of view. The bow shock appears to be steady from 800 μs onward, but the separated flow region does not reach a steady state until much later.

The images in Figs. 4e–4g are typical of images observed in the time interval from 1.4 to 3.0 ms. They are characterized by a steady bow shock (bs); however, the separation shock shape is slightly different from shot to shot. Variations in its shape are attributed to embedded shock waves, which are produced by supersonic flow deflected by turbulent eddies in the shear layer. The location and size of these turbulent eddies vary from shot to shot, thereby varying the location and strength of the embedded shocks. Consequently, the interaction of these shocks with the separation shock result in shot-to-shot variations in its shape. Figure 4g shows a particularly large-scale structure, which was observed at a delay time of 1800 μs. The appearance of such structures occurs randomly at different delay times.

After about 3.0 ms, the PLIF images become progressively darker with delay time as a result of diminishing NO concentration due to contamination and thus dilution by the driver gas. Further evidence of driver gas contamination at these delay times is the increase in the shock standoff distance, consistent with the accompanying increase in the ratio of specific heats.

Figures 5–8 show the various parameters defined in Fig. 2 measured from the PLIF images as a function of delay time. All distances are normalized to the fin diameter d of 38 mm, and all angles are measured in degrees from the plate surface.

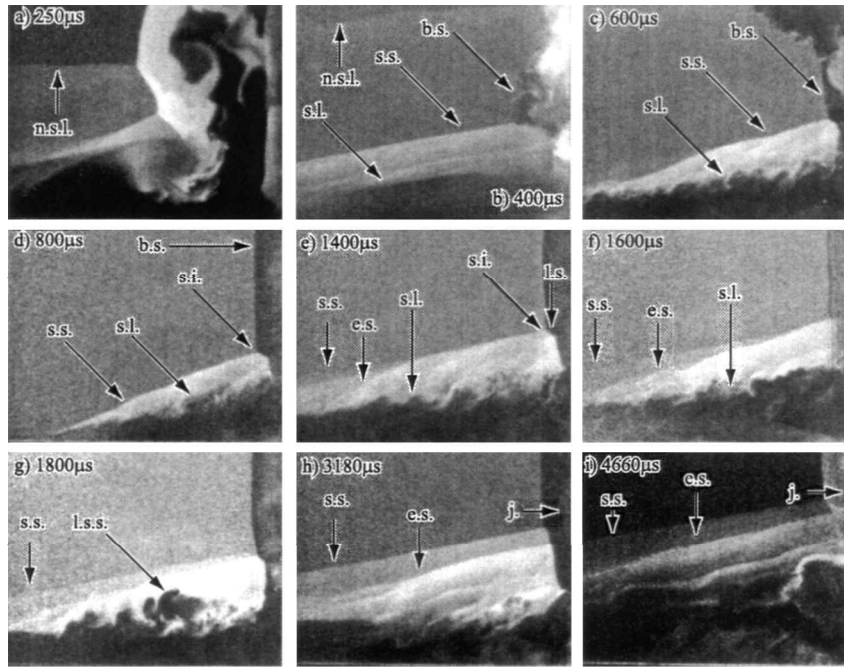

Fig. 4 PLIF images of the flow development where flow feature identified by letters: n.s.l., nozzle shear layer; b.s., bow shock; s.l., shear layer; l.s.s., large-scale structure; s.s., separation shock; e.s., embedded shock; s.i., shock-shock interaction; l.s., lambda shock; and j., jet produced by shock-shock interaction.

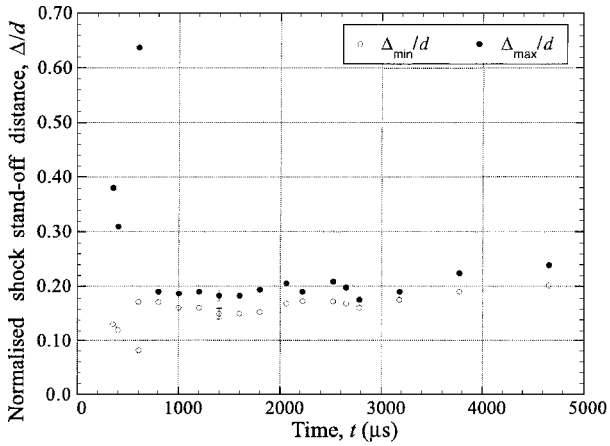

Fig. 5 Minimum and maximum bow-shock stand-off distances from the blunt fin normalized to blunt fin diameter.

Variation of the normalized bow shock standoff distance Δ/d with time is shown in Fig. 5. Both the minimum and maximum distance of the bow shock from the fin were recorded. This was considered necessary because the bow shock was not perfectly vertical in some of the images taken at earlier delays, (for example, see the bow shock shape at a time of 400 μs). The inviscid flow associated with the bow shock above the interaction region appears to stabilize after about 800 μs. The bow-shock standoff distance takes less time than other flow features to reach a steady value because it is an inviscid feature of the flow. According to Eq. (9), it takes only about 40 μs for the bow shock to establish on the fin at these conditions. Furthermore, at high Mach numbers, and in the absence of chemical effects, the shock standoff distance is only a weak function of Mach number. Hence, in the later stages of the nozzle flow establishment, it is quite insensitive to Mach number changes. If we assume that the measurements of the pitot pressure provide a good indication of the freestream Mach number during these later stages, the Mach number changes from about 5.9 at 800 μs to about 6.4 at 1500 μs. Based on Eq. (10) and the dependence of the density ratio on Mach number, the normalized shock standoff distance Δ/d will change by only a small amount. In fact, according to Eq. (10), it will change from 0.193 to 0.189 fin diameters over this Mach number range. The small change of 0.004 fin diameters is smaller than the uncertainty in our measurements, and hence, we expect the standoff distance to appear constant after 800 μs. This explains why the shock on the blunt fin appears to stabilize well before the flow at the exit of the nozzle has reached a constant Mach number. After about 3 ms, the bow shock standoff distance slowly increases as the gas composition of the flow changes due to the arrival of the driver gas. This increase in shock standoff distance is consistent with the dependence Δ/d of on the density ratio across the shock. The density ratio in turn depends on γ, which increases when the monatonic driver gas arrives.

Figure 6a shows how the vertical distance h_1 from the plate to the point of interaction between the bow and separation shocks and the angle of the separation shock, α_1, change with delay time. The point at which the separation shock intersects the flat plate occurs just outside the region of the PLIF images. An estimate of the separation length d_1, the distance from the blunt fin to the point where the boundary layer separates from the flat plate, can be obtained by extrapolating the separation shock to the point where it would have intersected the flat plate. This estimated separation length d_1, shown in Fig. 6b, settles to a value of approximately 4 fin diameters upstream of the fin during the steady flow time. This measurement assumes that the separation shock remains straight. CFD[37] indicates that near the point of separation this shock curves toward the flat plate, so measuring the value of d_1 by this method is an overestimate by about 10% determined by measuring the same shock angle repeatedly and averaging the results. However, in the image at a time of 800 μs, where the complete separation shock can be seen, there is no evidence of this curvature. From these results, we see that the size of the separated region (as characterized by the value of h_1) appears to stabilize after 1.5 ms. This time is significantly less than the conservative estimate of $\Delta t_{E,\max}$. In fact, we can now say that $\Delta t_E \approx \Delta t_{\text{nozzle}} = \Delta t_{E,\min}$. After approximately 3 ms, h_1 and d_1 increase and α_1 decreases due to the thickening of the boundary layer, caused by the decrease in flow pressure and possibly the arrival of the driver gas.

Previous schlieren and oil-flow measurements of d_1 for turbulent approaching boundary layers[27,38] have obtained values of d_1 that range between 2.5 and 3 fin diameters, whereas for fully laminar approaching boundary layers,[39] d_1 was measured at between 9 and 12 fin diameters. Thus, the present value of 4.0 is indicative of a

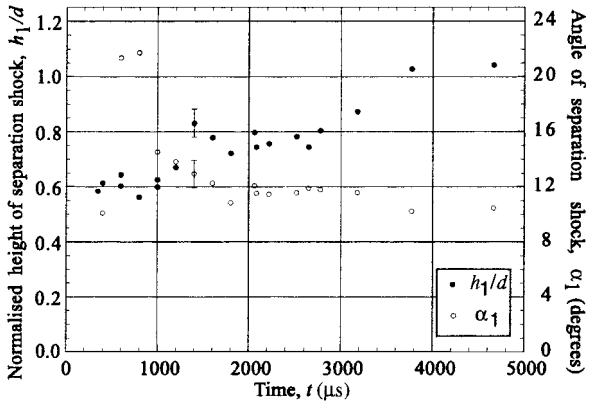

Fig. 6a Height from flat plate to point of interaction between separation shock and bow shock, and angle of the separation shock to the flat plate.

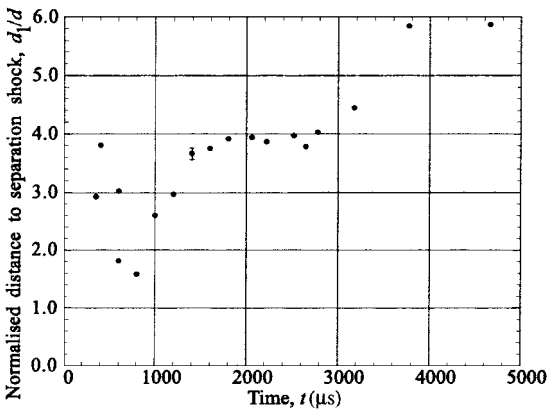

Fig. 6b Distance from the blunt fin to point of intersection of separation shock on the flat plate. (Parameters appear steady from ≈1.5 to 3.0 ms from shock reflection, giving some indication of when the inviscid interactions are stable.)

transitional approaching boundary layer. This is consistent with the measurements of He and Morgan,[30] which predict transition on a flat plate at a freestream Reynolds' number of approximately 1×10^6, which, for this flow condition, occurs 170 mm downstream of the leading edge, near the position of TC2.

The results of our measurements of h_2 and d_2 are shown in Fig. 7. The distance d_2 from the blunt fin to the point of intersection of the shear layer with the flat plate is estimated in the same way as the separation length d_1 described earlier. The uncertainty in the average position of d_2 is greater than that for d_1 because of the turbulent nature of the shear layer. Figure 7a shows h_2 and the angle of the shear layer, α_2, as a function of delay time. The measured value of d_2, is shown in Fig. 7b. At early delays, $d_2 \approx d_1$. Both values decrease as the separation point moves slowly toward the blunt fin before the steady flow time. They then both increase as it moves away from the blunt fin again at later times. At these later times, the values of d_1 and d_2 differ significantly from each other with $d_1 > d_2$. The value of h_2 does not vary much as a function of time and stays between about 0.4 and 0.6 fin diameters throughout the flow time.

The angle of the lambda shock, α_λ, shows an oscillatory behavior that persists even during the time when the separation shock and shear layer appear to be steady, as shown in Fig. 8. Superimposed on the oscillatory behavior, the value of α_λ shows a tendency to increase with time.

In summary, the images show that the start of the steady flow time is at approximately 1500 μs, which is consistent with the value of $\Delta t_{E,\min}$ as discussed earlier.

Heat Flux

For comparison with the PLIF images and to further increase our understanding of the flow establishment processes, surface temper-

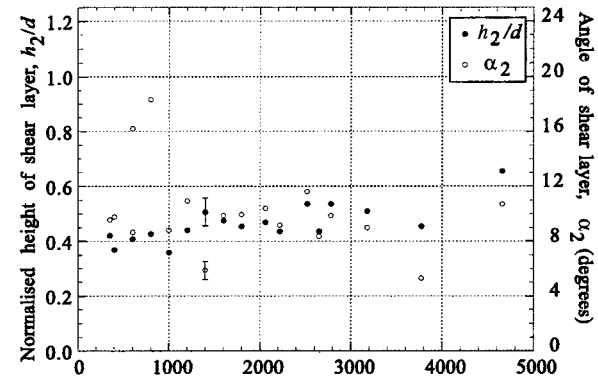

Fig. 7a Height from flat plate to point of interaction between shear layer and bow shock and angle of the shear layer shock to the flat plate.

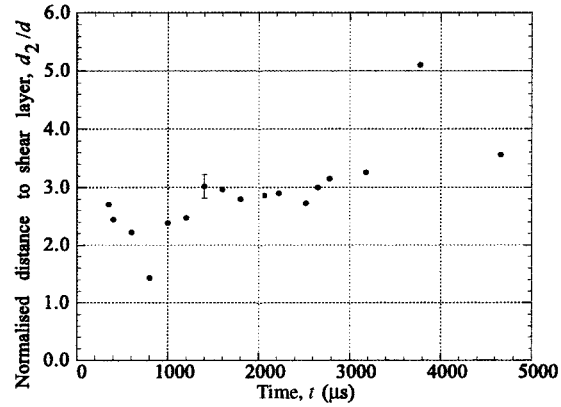

Fig. 7b Distance from blunt fin to point of intersection of shear layer on the flat plate. (Inviscid part of the flow appears to be steady from ≈1.5 to 3.0 ms.)

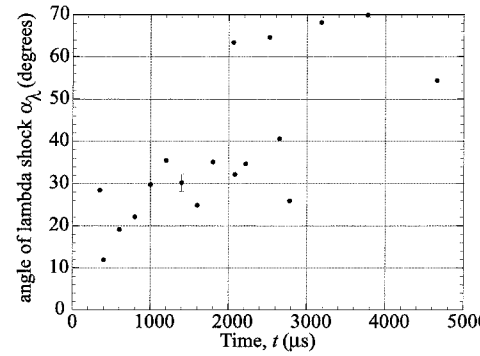

Fig. 8 Angle of lambda shock to the horizontal.

ature measurements were obtained for three tunnel runs at the same flow condition as the PLIF images. An additional measurement was obtained for flow along the flat plate in the absence of the fin. The comparison between the two heat flux measurements indicates the effect of the blunt fin on the flow.

The surface heat flux time histories $\dot{q}_s(t)$ for the four thermocouples are shown in Fig. 9. Each plot is for one thermocouple. The raw data from each thermocouple has been analyzed in the manner described by Diller[40] and Mallinson et al.[19] to produce the heat flux measurements shown in Fig. 9. Two plots show the heat flux with and without the blunt fin. The plots show the effect of the fin on the upstream heat flux. Each trace contains an initial heat flux spike, followed by a period of unsteady heat flux corresponding to the initial shock and unsteady expansion in the hypersonic nozzle starting shock system process, as described by Smith.[20] This is followed by a period of decreasing heat flux as the boundary layer on the plate establishes itself. The heat flux maintains a roughly steady value from 1.4 to 2.5 ms, followed by a roughly linear decrease in heat

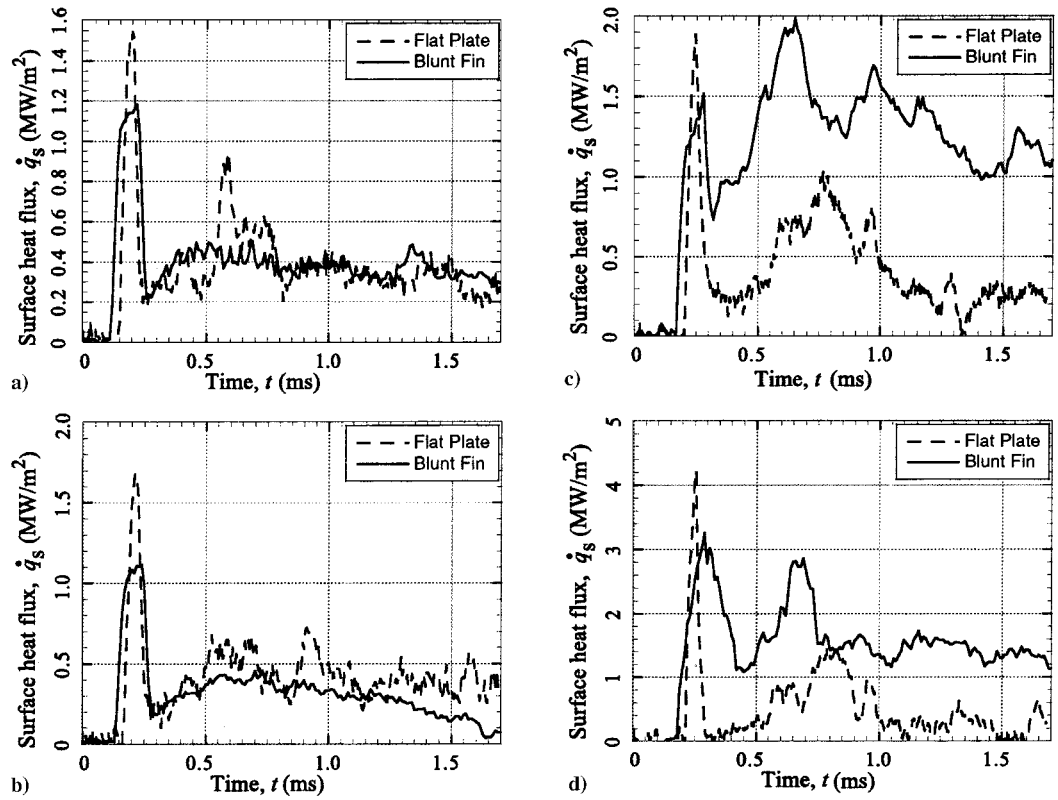

Fig. 9 Flat plate without the blunt fin present and average time history of surface heat flux for a) TC1, b) TC2, c) TC3, and d) TC4.

flux caused by decreasing nozzle-reservoir pressure and contamination of the test gas by the helium driver gas. (Only the first 1.7 ms are shown in Fig. 9; the first 4.0 ms of the surface heat flux history is shown subsequently.)

Figure 9a shows that the heat flux at TC1 is the same for both the flat plate and the blunt fin flows during the steady flow time. This indicates that the separation has no measurable influence this far upstream. TC2, shown in Fig. 9b, measures less heat flux for the blunt fin than for the flat plate. This is due to the decrease in skin friction immediately upstream of separation, which is related to the heat flux via the Reynolds' analogy

$$St = C_f/2(Pr)^{\frac{2}{3}} \tag{11}$$

Figure 6b places the separation point at 4 fin diameters, or 152 mm, upstream of the fin. Because the measurement of d_1 is a linear extrapolation of the separation shock, this may be a slight overprediction, but should be close to the actual separation point. TC2 is located 153 mm upstream of the fin, which should be less than 10 mm upstream of the point of separation.

Figure 9c and 9d, which display the heat flux traces for TC3 and TC4, respectively, show much higher heat flux rates for the blunt fin than for the flat plate, due to surface heating caused by flow reattachment in front of the fin. The general shape of the heat flux trace upstream of the fin is similar to that measured by Schuricht and Roberts[41] for the laminar boundary layer upstream of a blunt fin in a hypersonic freestream.

The effect of the presence of the blunt fin on the heat flux can be readily seen in Fig. 10, which displays a plot of Stanton number against Reynolds number. The Stanton number St is calculated using

$$St = \frac{\dot{q}_s(t)}{\rho_e u_e \left[h_e + (Pr)^{0.5}\left(0.5 \cdot u_e^2\right) - h_w\right]} \tag{12}$$

where ρ_e, u_e, and h_e are the density, velocity and enthalpy of the freestream outside the boundary layer, as calculated by STUBE, and h_w is the enthalpy at the wall. For the flat plate, the data fall on a straight line. For the blunt fin measurements, TC1 follows the flat plate heat flux, TC2 decreases relative to the flat plate value as

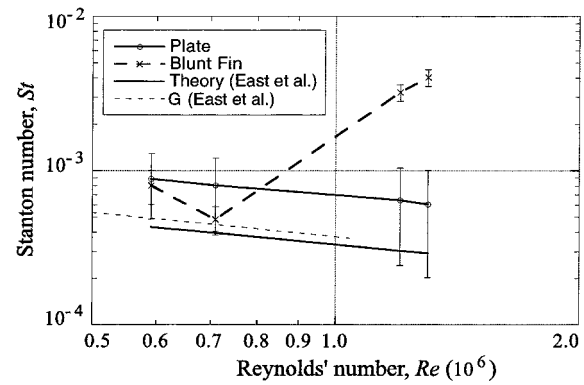

Fig. 10 Stanton number vs Reynolds number shows effect of blunt fin on the heat transfer.

discussed earlier, whereas there is an increase in heat flux over the flat plate value of 4 to 5 times for TC3 and TC4.

Also included in Fig. 10 are the data from East et al.[42] for their condition G measurements made using a flat plate of identical dimensions to that used in this study and at similarly low stagnation enthalpy (2.79 MJ/kg). The data obtained in this experiment have the same slope as that measured by East et al., and the condition G results fall within the error bars for our measurement, but the Stanton number of the present result is measurably higher. Both results were obtained in the same facility, in perfect gas flows. The only difference between the heat flux measurements was that East et al. used thin film gauges rather than the thermocouples used in these experiments. There may be some small systematic difference between measurements using these two techniques. More data would need to be acquired to reduce the uncertainty of the present series of measurements before we could be sure that the difference is truly systematic. The measured Stanton number is also higher than the theoretical relation quoted by East et al., which is a simple Blasius boundary-layer and Reynolds analogy approximation that predicts $St\sqrt{Re} = 0.332$. The systematic difference between measured values and the theoretical relationship is probably due to the theory not

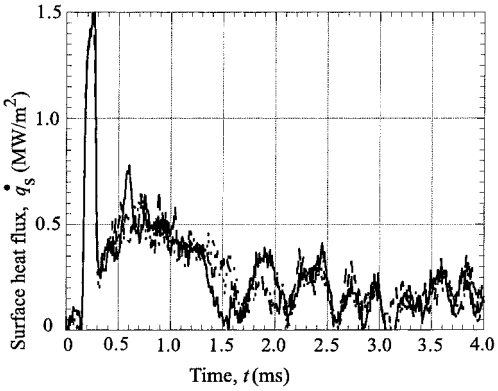

Fig. 11 Example of the oscillatory behavior of surface heat flux shown by three sets of results (solid line, dashed line, dotted line) for thermocouple TC2, showing the repeatability of the result due to a dynamic equilibrium between filling and release of fluid in the separated region upstream of the fin, analogous to the vortex shedding found in subsonic wake flows.

accounting for the pressure gradient along the plate or the density variation across the boundary layer.

The heat flux measured by TC2 also exhibited strongly oscillatory behavior in the presence of the blunt fin, which was not apparent in the flat plate flow. This is clearly shown by the three sets of heat flux distributions presented in Fig. 11. Approximately 1.5 ms after shock reflection, the heat flux oscillates at a frequency of 2.0 ± 0.2 kHz or 3.6 ± 0.3 kHz. The three traces indicate that this behavior is repeatable. The oscillation has been observed and measured in other experiments using wavelet transform techniques[43] and is due to a dynamic equilibrium between filling and release of fluid in the separated region upstream of the fin, analogous to the vortex shedding found in subsonic wake flows. The temporal resolution of the PLIF survey was of the same order as the oscillation frequency, and so the effect of these oscillations was not seen in the images. The similarity of the images obtained between 1.4 and 3 ms after shock reflection suggests that small fluctuations in the position and angle of the separation shock may have a significant effect on the plate heat flux. Care must be exercized when interpreting visual indications of flow steadiness, particularly in inherently oscillatory flows. The fact that 3–4 oscillations occur during the test time give us some confidence in saying that, in this case, the flow has reached a steadily oscillating state approximately 2 ms after shock reflection.

Uncertainties

The uncertainty in the pitot and nozzle reservoir pressure measurements is largely a result of shot noise, which is readily visible in the pressure histories shown in Fig. 3. This noise, which is significantly larger than the systematic uncertainty caused by the uncertainty in transducer sensitivity, is approximately $\pm 2\%$ for the nozzle reservoir pressures and approximately $\pm 5\%$ for the pitot pressures. The resultant uncertainty in the pressure ratio is, thus, approximately $\pm 6\%$.

The uncertainty in each parameter specifying the freestream flow condition is a result of the uncertainties in the input parameters used by the STUBE[23] code, which models the nozzle flow and calculates the freestream condition. The input parameters are the measured speed of the primary shock and the measured value of the nozzle reservoir pressure.[22] The uncertainty in the measured shock speed is less than $\pm 1\%$, whereas the standard deviation in the shot-to-shot scatter of the shock speed is determined to be approximately $\pm 2\%$. The uncertainty in the measurement of the nozzle reservoir pressure for steady flow conditions is approximately $\pm 2\%$, whereas the standard deviation in the shot-to-shot scatter is determined to be approximately $\pm 4\%$.

For the results displayed in Figs. 5–8, the uncertainty in the measurements of Δ, h_1, h_2, α_1, α_2, and α_λ are largely a result of spatial resolution limitations of the PLIF images. In the case of measurements of d_1 and d_2, an additional contribution to the uncertainty arises from the linear exptrapolation. Measurements involving the shear layer, such as those for d_2 and h_2, are additionally affected by its turbulent nature, which causes its shape and location to be ill defined. The perturbation of the separation shock by interactions from the embedded shock waves cause its shape to change slightly from shot to shot, which results in scatter of the values of d_1 and h_1. An estimate of the scatter of d_1, d_2, h_1, and h_2 was made from measurements of these values for 15 different images at a delay time of 1400 μs. The standard deviation of this scatter added in quadrature with the uncertainty of an individual measurement for a parameter is used to estimate the overall uncertainty for that parameter, which is displayed in terms of an error bar at a delay time of 1400 μs for Figs. 5–8.

The uncertainty in determining the nozzle flow establishment time from the pressure ratio shown in Fig. 3 is estimated from the slope of this ratio as compared with its uncertainty. From these considerations, an uncertainty of ± 50 μs is attributed to the determination of nozzle establishment time.

The uncertainty in the surface heat flux depends on the noise in the raw thermocouple signals and the average signal level. For the flat plate experiments, the uncertainties in the heat flux measurements are quite large because of the low signal levels and because the results involved measurements from only a single shot. In particular, for the flat plate, the relative uncertainties in heat fluxes measured by the four thermocouples at a delay time of 1.4 ms are as follows: TC1 $\pm 50\%$, TC2 $\pm 40\%$, TC3 $\pm 60\%$, and TC4 $\pm 66\%$. For the blunt-fin experiment, the uncertainties are significantly smaller because of higher signals and shot averaging. Furthermore, for the blunt-fin experiments, improvements were made to reduce the noise level of the amplifiers. Based on the average of three shots, it is found that, at delay time of 1.4 ms, the relative uncertainties in thermocouples in the blunt-fin experiments are as follows: TC1 $\pm 25\%$, TC2 $\pm 20\%$, TC3 $\pm 14\%$, and TC4 $\pm 12\%$.

Conclusions

PLIF has been successfully used to visualize the development of the separated region upstream of a blunt fin on a sharp-nosed flat plate at zero incidence in a hypersonic freestream. The images indicate that, for the flow conditions studied, the separated flow region establishes within about 1.5 ms and that nominally steady flow conditions persist for at least an additional 1.5 ms. Heat flux results indicate a similar starting time, but also exhibit oscillatory behavior, which continues throughout the test time. The test time is sufficiently long lived to allow 3–4 oscillations to occur. These results indicate that this type of quasi-steady viscous interaction problem can be studied successfully despite the limited test times of the free-piston shock tunnel.

The measured distance from the fin to the separation point is consistent with a transitional flow, situated between previously measured values for flows having turbulent and laminar approaching boundary layers. The heat flux distribution during the test time shows undisturbed upstream flow, a reduction in heat flux close to the separation point, and heat flux of 4–5 times the flat plate value downstream of separation.

Acknowledgments

This study was carried out as part of a research program supported by a Faculty Research Grant funded through the Australian National University. The valuable discussions of this work before and during experiments with Charles Hill and Matthew Gaston are gratefully acknowledged. The authors wish to thank Paul Walsh for the contribution of his technical expertise in this project.

References

[1] Korkegi, R. H., "Survey of Viscous Interactions Associated with High Mach Number Flight," *AIAA Journal*, Vol. 9, No. 5, 1971, pp. 771–783.

[2] Stollery, J. L., "Some Aspects of Shock-Wave Boundary-Layer Interaction at Hypersonic Speed," *Proceedings of the 17th International Symposium on Shock Waves and Shock Tunnels*, American Inst. of Physics, New York, 1989, pp. 12–22.

[3] Neumann, R. D., and Hayes, J. R., "Protuberance Heating at High Mach Numbers—A Critical Review and Extension of the Database," AIAA Paper 81-0420, Jan. 1981.

[4] McMaster, D. L., and Shang, J. S., "A Numerical Study of Three-Dimensional Separated Flows Around a Sweptback Blunt Fin," AIAA Paper 88-0125, Jan. 1988.

[5]Stollery, J. L., "Some Aspects of Shock-Wave Boundary-Layer Interaction Relevant to Intake Flows," *Aerodynamics of Hypersonic Lifting Vehicles*, CP-428 AGARD, 1987.

[6]Kussoy, M. I., and Horstman, K. C., "Three-Dimensional Hypersonic Shock Wave/Turbulent Boundary-Layer Interactions," *AIAA Journal*, Vol. 31, No. 1, 1993, pp. 8, 9.

[7]Knight, D. D., Horstman, C. C., Shapey, B., and Bogdonoff, S., "Structure of Supersonic Turbulent Flow Past a Sharp Fin," *AIAA Journal*, Vol. 25, No. 10, 1987, pp. 1331–1337.

[8]Settles, G., and Teng, H. Y., "Flow Visualization of Separated Three-Dimensional Shock Wave/Turbulent Boundary-Layer Interactions," *AIAA Journal*, Vol. 21, No. 3, 1983, pp. 390–397.

[9]Roberts, G. T., and East, R. A., "Liquid Crystal Thermography for Heat Transfer Measurement in Hypersonic Flows: A Review," *Journal of Spacecraft and Rockets*, Vol. 33, No. 6, 1996, pp. 761–768.

[10]Roberts, G. T., Schuricht, P. H., and Mudford, N. R., "Heating Enhancement Caused by a Transverse Control Jet in Hypersonic Flow," *Shock Waves Journal*, Vol. 8, No. 2, 1998, pp. 105–112.

[11]Watson, R. D., and Weinstein, L. M., "A Study of Hypersonic Corner Flow Interactions," AIAA Paper 70-227, Jan. 1970.

[12]Garrison, T. J., Settles, G. S., Narayanswami, N., and Knight, D. D., "Structure of Crossing Shock-Wave/Turbulent-Boundary-Layer Interactions," *AIAA Journal*, Vol. 31, No. 12, 1993, pp. 2204–2211.

[13]Settles, G. S., and Dobson, L., "Supersonic and Hypersonic Shock/Boundary-Layer Interaction Database," *AIAA Journal*, Vol. 32, No. 7, 1994, pp. 1377–1383.

[14]Olejniczak, J., and Candler, G. V., "Computation of Hypersonic Shock-Interaction Flow Fields," AIAA Paper 98–2446, June 1998.

[15]Amaratunga, S. R., Tutty, O. R., and Roberts, G. T., "Computations of Laminar, High Enthalpy Air Flow over a Compression Ramp," SP 426, ESA, 1999, pp. 213–220.

[16]Olejniczak, J., Candler, G. V., Wright, M. J., Hornung, H. G., and Leyva, I. A., "High-Enthalpy Double-Wedge Experiments," AIAA Paper 96-2238, 1996.

[17]Stalker, R. J., "Development of a Hypervelocity Wind Tunnel," *Aeronautical Journal*, Vol. 76, No. 738, 1972, pp. 374–384.

[18]O'Byrne, S. B., Houwing, A. F. P., and Danehy, P. M., "Establishment of the Near-Wake Flow of a Cone and Wedge in a Transient Hypersonic Freestream," *Proceedings of 22nd International Symposium on Shock Waves*, Univ. of Southampton, Southampton, England, U.K., 1999, pp. 1583–1588.

[19]Mallinson, S. G., Gai, S. L., and Mudford, N. R., "The Interaction of a Shock Wave with a Laminar Boundary Layer at a Compression Corner in High-Enthalpy Flows Including Real-Gas Effects," *Journal of Fluid Mechanics*, Vol. 342, No. 10, 1997, pp. 1–35.

[20]Smith, C. E., "The Starting Process in a Hypersonic Nozzle," *Journal of Fluid Mechanics*, Vol. 24, No. 4, 1966, pp. 625–640.

[21]Saito, T., and Takayama, K., "Numerical Simulations of Nozzle Starting Process," *Shock Waves Journal*, Vol. 9, No. 2, 1999, pp. 73–79.

[22]Boyce, R. R., Morton, J. W., Houwing, A. F. P., Mundt, C., and Bone, D. J., "Computational Fluid Dynamics Validation Using Multiple Interferometric Views of a Hypersonic Flowfield," *Journal of Spacecraft and Rockets*, Vol. 33, No. 3, 1996, pp. 319–325.

[23]Vardavas, I. M., "Modelling Reactive Gas Flows Within Shock Tunnels," *Australian Journal of Physics*, Vol. 37, No. 2, 1984, pp. 157–177.

[24]Davies, W., and Bernstein, J., "Heat Transfer and Transition to Turbulence in the Shock-Induced Boundary Layer on a Semi-Infinite Flat Plate," *Journal of Fluid Mechanics*, Vol. 36, No. 1, 1969, pp. 87–112.

[25]Holden, M. S., "Establishment Time of Laminar Separated Flows Within Shock Tunnels," *AIAA Journal*, Vol. 9, No. 11, 1971, pp. 2296–2298.

[26]Eckert, E. R. G., "Engineering Relations for Friction and Heat Transfer to Surfaces in High Velocity Flow," *Journal of Aeronautical Science*, Vol. 22, No. 8, 1955, pp. 585–587.

[27]Westkaemper, J. C., "Turbulent Boundary Layer Separation Ahead of Cylinders," *AIAA Journal*, Vol. 6, No. 7, 1968, pp. 1352–1355.

[28]Miles, J. W., Mirels, H., and Wang, H. E., "Time Required for Establishing a Detached Bow Shock," *AIAA Journal*, Vol. 4, No. 6, 1966, pp. 1127–1128.

[29]Hornung, H. G., "Non-equilibrium Dissociating Nitrogen Flow over Spheres and Circular Cylinders," *Journal of Fluid Mechanics*, Vol. 53, No. 1, 1972, pp. 149–176.

[30]He, Y., and Morgan, R. G., "Transition of Compressible High Enthalpy Boundary Layer Flow over a Flat Plate," *Aeronautical Journal*, Vol. 98, No. 2, 1994, pp. 25–33.

[31]Houwing, A. F. P., Palmer, J. L., Thurber, M. C., Wehe, S. D., Hanson, R. K., and Boyce, R. R., "Comparison of Planar Fluorescence Measurements and Computational Modeling of a Shock Layer Flow," *AIAA Journal*, Vol. 34, No. 3, 1996, pp. 470–477.

[32]Hiller, B., and Hanson, R. K., "Simultaneous Planar Measurements of Velocity and Pressure Fields in Gas Flows Using Laser-Induced Fluorescence," *Applied Optics*, Vol. 27, No. 1, 1988, pp. 33–48.

[33]Fox, J. S., Gaston, M. J., Houwing, A. F. P., Danehy, P. M., Mudford, N. R., and Gai, S. L., "Instantaneous Mole-Fraction PLIF Imaging of Mixing Layers Behind Hypermixing Injectors," AIAA Paper 99-0774, 1999.

[34]McIntyre, T. J., Houwing, A. F. P., Palma, P. C., Rabbath, P., and Fox, J. S., "Imaging of Combustion in a Supersonic Combustion Ramjet," *Journal of Propulsion and Power*, Vol. 13, No. 3, 1997, pp. 388–394.

[35]Hill, C. D., Danehy, P. M., Fox, J. S., Houwing, A. F. P., and Gaston, M. J., "Instantaneous Temperature Imaging in a Free-Piston Shock Tunnel," *Proceedings of 2nd Australian Conference on Laser Diagnostics in Fluid Mechanics and Combustion*, Monash Univ., Melbourne, Australia, 1999, pp. 109–110.

[36]Palma, P. C., Houwing, A. F. P., and Sandeman, R. J., "Absolute Intensity Measurements of Impurity Emissions in a Shock Tunnel and Their Consequences for Laser Induced Fluorescence Experiments," *Shock Waves Journal*, Vol. 3, No. 1, 1993, pp. 49–53.

[37]Hung, C. M., and Buning, P., "Simulation of Blunt-Fin-Induced Shock-Wave and Turbulent Boundary Layer Interaction," *Journal of Fluid Mechanics*, Vol. 154, May 1985, pp. 163–185.

[38]Dolling, D. S., and Bogdonoff, S. M., "Blunt Fin-Induced Shock Wave/Turbulent Boundary-Layer Interaction," *AIAA Journal*, Vol. 20, No. 12, 1978, pp. 1674–1680.

[39]Hung, F. T., and Clauss, J. M., "Three Dimensional Protuberance Interference Heating in High-Speed Flow," AIAA Paper 80-0289, 1980.

[40]Diller, T. E., "Advances in Heat Flux Measurements," *Advances in Heat Transfer*, Vol. 23, No. 1, 1993, pp. 279–368.

[41]Schuricht, P. H., and Roberts, G. T., "Hypersonic Interference Heating Induced by a Blunt Fin," AIAA Paper 98–1579, 1998.

[42]East, R. A., Stalker, R. J., and Baird, J. P., "Measurement of Heat Transfer to a Flat Plate in a Dissociated High-Enthalpy Laminar Air Flow," *Journal of Fluid Mechanics*, Vol. 97, No. 4, 1980, pp. 673–699.

[43]Poggie, J., and Smits, A. J., "Wavelet Analysis of Wall-Pressure Fluctuations in a Supersonic Blunt-Fin Flow," *AIAA Journal*, Vol. 35, No. 10, 1997, pp. 1597–1603.

R. P. Lucht
Associate Editor